An Experimental Investigation of Microbubble Generation in a Confined Turbulent Jet

P.A. Brandner[1], G. Wright[2] B. Pearce[1], L. Goldsworthy[1] and G.J. Walker[3]

[1]Australian Maritime College, University of Tasmania
Launceston, Tasmania 7250, Australia

[2]Maritime Platforms Division, Defence Science and Technology Organisation,
Fishermans Bend, Victoria 3032, Australia

[3]School of Engineering, University of Tasmania
Hobart, Tasmania 7001, Australia

Abstract

Microbubbles generated from the expansion of water supersaturated with dissolved air through a sharp edged orifice are investigated using shadowgraphy. Demineralised water saturated to an equilibrium concentration corresponding to 5 atmospheres is expanded through a 0.5 mm diameter × 0.3 mm thick orifice plate into a 1.2 mm diameter tube at atmospheric pressure. Cavitation occurrence in the small-scale turbulent structures combined with gaseous diffusion promotes the formation of microbubbles. The length of the tube downstream of the orifice is 200 mm. This length affects bubble coalescence and hence the number and size of bubbles ejected. To enable measurements of bubble size and volumetric concentration the ejected bubbly plume is dispersed in a co-flowing stream of fine-scale turbulence to achieve a homogeneous distribution in a transparent duct through which shadowgraphy measurements can be made. The bubble shadows are created using diffused laser backlighting viewed with a CCD camera via a long range microscope.

Introduction

Processes using microbubbles have diverse areas of application including mineral processing, water treatment, medicine and in the present context for experimental modelling of cavitation and bubbly flows [4,11,14].

Populations of minute bubbles are present in all practical volumes of water, controlling the inception and dynamics of cavitation phenomena [4,6,10]. These bubbles provide sites for nucleation and the inception of phase change. Such microbubbles or nuclei have a critical pressure, depending on diameter, below which their equilibrium is unstable thus undergoing rapid growth and hence leading to complex macroscopic cavitation phenomena [1]. The critical pressure is always less than the vapour pressure, decreasing with bubble diameter such that for small or micron sized bubbles large liquid tensions (negative pressures) are required for cavitation inception.

In hydrodynamic research, in addition to cavitation phenomena, there is also interest in the physics of microbubble formation and dispersion about the hulls, propulsors and appendages of marine vehicles [7]. Microbubbles also introduce the possibility of providing soluble seeding for diagnostic techniques such as Particle Imaging Velocimetry (PIV).

The new variable-pressure water tunnel recently completed as part of the Cavitation Research Laboratory (CRL) at the Australian Maritime College (AMC) has been developed with the capability for continuous injection and separation of microbubbles [2,3]. This capability, necessary for rigorous modelling of basic cavitation and bubbly flow physics, was incorporated into the facility design from the beginning of the planning process. The system was developed on the basis that it must be capable of homogeneous seeding of the flow with a range of microbubbles sizes, at concentrations ranging over several orders of magnitude and be of sufficiently small scale to be incorporated upstream of the contraction without unduly influencing the test section flow.

Various methods for the generation of microbubbles are available with new methods being developed on an ongoing basis [10,13,14]. The method chosen is reported by Lecoffre [10] and involves the expansion of water supersaturated with dissolved air through a small sharp edged orifice into a small diameter tube. Such small scale devices may be distributed over the cross-section of the settling chamber supported on relatively thin hydrofoil sections traversing the tunnel ductwork. The final realisation of the system involves 100 'mini-tube' type generators arranged on a 10 × 10 array to uniformly seed the flow. Detailed descriptions of the nuclei injection system implemented in the CRL water tunnel are given in [2,3].

Details of the mini-tube type microbubble generator are shown in figure 1. Water supersaturated with dissolved air is supplied via a 3.2 mm diameter tube and expanded through a 0.5 mm diameter × 0.3 mm thick orifice plate into a 1.2 mm diameter tube from the equilibrium saturation pressure to external pressure. Cavitation occurrence in the small-scale turbulent structures combined with gaseous diffusion promotes the formation of microbubbles. The length of the tube downstream of the orifice is 200 mm. This length affects bubble coalescence and hence the number and size of bubbles ejected. As part of the commissioning of the CRL water tunnel the nuclei generators are being characterised to determine the size and production rates of bubbles generated as a function of the orifice and tube geometric and operational parameters.

A diverse range of methods has been developed for the measurement of microbubble or nuclei spectra in test facilities [10]. The present study reports on the development of an experimental setup utilising shadowgraphy for the measurement of generated bubble sizes and production rates. To enable measurements of bubble size and volumetric concentration the ejected bubbly plume is dispersed in a co-flowing stream of fine turbulence to achieve a homogeneous distribution in a transparent duct through which shadowgraphy measurements can be made. The bubble shadows are created by backlighting with diffused laser light, viewed with a CCD camera via a long range microscope.
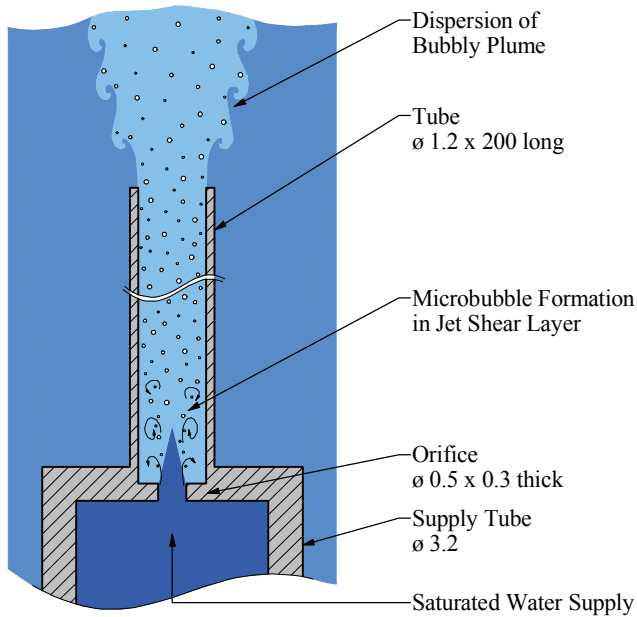
Figure 1. Details of the mini-tube type microbubble generator used for the present study (as implemented in the Australian Maritime College Cavitation Research Laboratory water tunnel). All dimensions in mm.

Experimental Overview

Experimental Set-up

The shadowgraphy experiments were carried out using the Bubble Dynamics Chamber (BDC)—a, variable pressure chamber designed for investigating small-scale bubble and cavitation phenomena in the CRL. Figure 2 shows a schematic of the experimental setup. The BDC has a test volume of 520 mm × 520 mm × 1200 mm, is constructed of 46 mm thick stainless steel plates with optical access on the 4 long sides through 1020mm × 350mm × 85mm thick acrylic windows. The BDC has the same operating pressure range as the CRL water tunnel—4 to 400kPa absolute. The working fluid for both the BDC and the microbubble generation system is demineralised water with conductivity of order 1 μS/cm.

A secondary circuit installed within the BDC permits the continuous dilution and homogeneous dispersion of the generated microbubble plume, as shown in figures 2 and 3. The section of circuit passing through the BDC is a 60 mm square internal cross-section × 8 mm thick glass duct. The dilution flow may be adjusted to vary the bubble concentration which is a trade-off between higher concentrations to capture a greater number of bubbles per image as opposed to less background interference at lower concentrations. An initially uniform, parallel and low turbulence flow is created 25mm upstream from the point microbubble injection using gauzes and a honeycomb. A gauze is located after the mitre bend where the mini-tube penetrates the circuit. Another similar gauze and a honeycomb are located after the round to square transition just upstream of the glass duct, as shown in figure 2.

The mixed bubbly flow is discharged radially from the glass duct at the top of the BDC below a free surface to enhance bubble separation. The dilution flow is drawn from a nozzle near the bottom of the BDC ensuring that no bubbles are ingested for runtime limits of about 60 s. With this arrangement it is possible to carry out experiments over the full range of BDC operating pressures. For the present work however the BDC was maintained at atmospheric pressure. The dilution flow rate is measured using a Great Plains Industries Model 075E liquid turbine meter with a precision < ±0.5%.
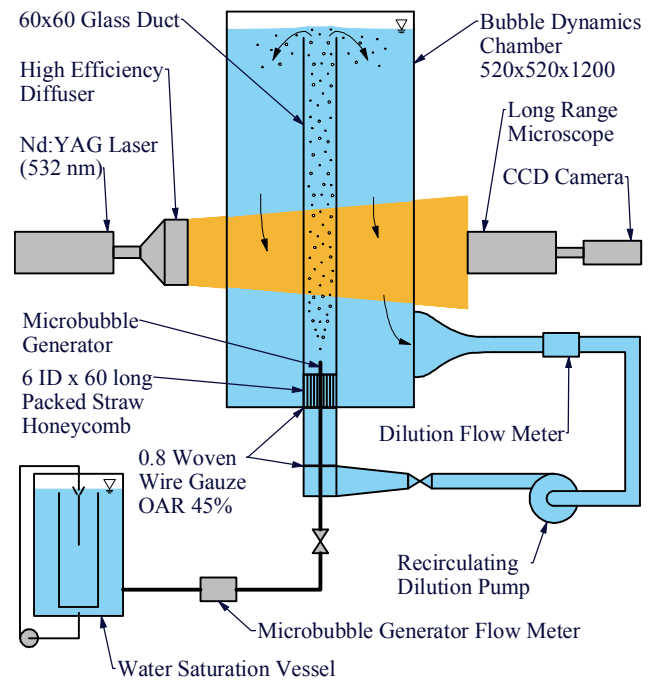

Figure 2. Schematic of experimental set-up of Bubble Dynamics Chamber (BDC) for measurement of microbubble size and production rate. Generated microbubbles are mixed in a dilution flow within a central glass duct to give a homogeneous dispersion. Microbubbles are imaged using shadowgraphy on the centreline of a glass duct. All dimensions in mm.
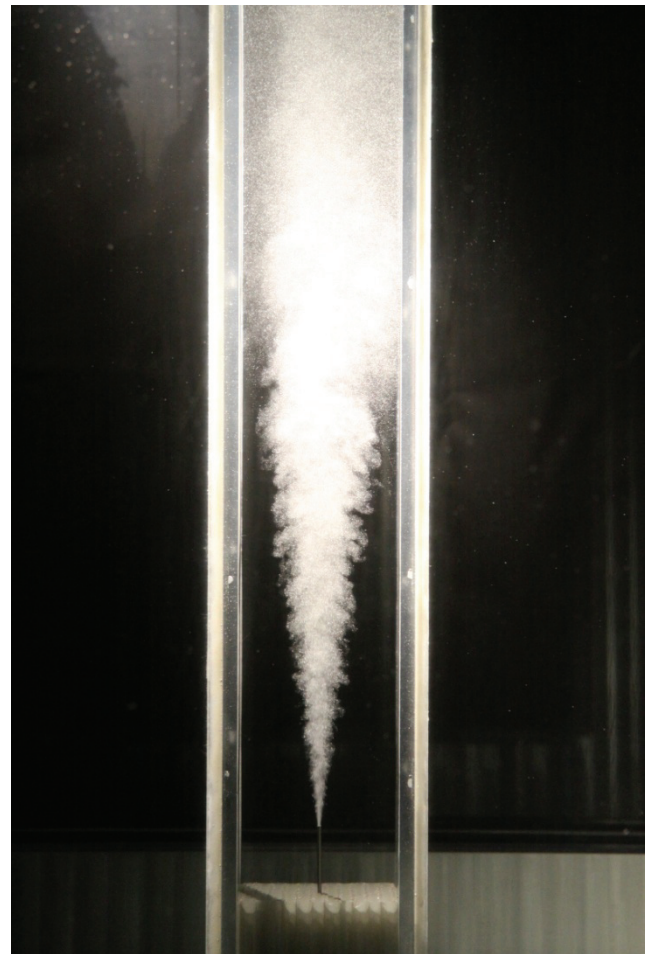

Figure 3. Mixing and dispersion of injected microbubbles in recirculating dilution flow.

Supersaturated water is supplied to the microbubble generator from a saturation vessel that may be pressurised to 2000 kPa. To rapidly saturate an initially filled vessel an ancillary circuit is used. Vessel water is recirculated through a venturi with a perforated throat to ingest air from above the free surface enhancing the dissolution process. The saturation vessel pressure is measured using a Wika gauge pressure transducer Model P-10 with a precision of 0.1%. Atmospheric pressure is measured using a Vaisala Model PTB210 digital barometer with precision of ±0.03 kPa. The dynamic dissolved O_2 concentration and temperature during initial saturation are measured using a Hach Ultra Orbisphere Model A1100 EC dissolved O_2 sensor. The equilibrium dissolved O_2 concentration is also estimated using empirical relations and tabulated data [12]. The flow of supersaturated water to the microbubble generator is measured using the time rate of change of a level sensor from data acquired by a standard National Instruments/LabView data acquisition system. The level sensor is an Orion Instruments magnetically coupled liquid level sensor. The estimated precision of the microbubble generator flow rate measurement is < ±0.5%.

The optical axis for the present measurements was located 550 mm downstream from the point of microbubble injection. This location was chosen on the basis of being sufficiently far downstream for the bubbles to be homogeneously mixed but not too far for significant coalescence or dissolution to occur.

The shadowgraphy set-up used is part of a LaVision shadowgraphy and stereo PIV system. The backlighting for the shadowgraphy is from diffused laser light sourced from a 120mJ Litron Nano L PIV Nd:YAG (532 nm) laser diffused through a LaVision high efficiency diffuser using a fluorescent dye plate. Light pulses emitted from the diffuser are in the wavelength range 574 to 580 nm and of 20 ns duration when excited by 532 nm wavelength laser pulses of 5 ns duration.

Images were captured using a LaVision Image Intense PIV camera via a Questar QM1 long range microscope. The CCD in the camera is 1376 pixels wide × 1040 pixels high with 12 bit optical resolution. The long range microscope was coupled to the camera using a 3× Barlow lens to enable a field of view of 975 μm × 733 μm giving a spatial resolution of 0.71 μm/pixel. This magnification was chosen based on expectations of sizing bubbles down to 10 μm diameter.

The laser and camera were triggered from a programmable timing unit and shadowgraphy analysis was carried out using LaVision DaVis Version 7.2 software.

Experimental Procedure

As there is no requirement for measurement of bubble velocities in the present work the camera and laser were operated in single frame mode. This enabled a repetition rate of 10 Hz and about 545 images to be acquired over a single run of about 50 s. For the present work 10 runs were made giving a total of 5397 images for analysis.

Quantities measured continuously during each 50 s runtime included the microbubble generator liquid flow rate, the dilution flow rate, the atmospheric pressure and the saturation vessel gauge pressure. Quantities measured at the beginning of each run included the BDC water temperature and the saturation vessel water temperature and dissolved O_2 concentration.

For the present initial work only one saturation vessel pressure and BDC pressure (or cavitation number) were investigated. The relevant dimensionless parameters characterising the microbubble generator flow are the cavitation number, $\sigma = (p_2 - p_v)/(p_1 - p_2)$, Weber number, $We = \rho U^2 d/S$ and Reynolds number, $Re = Ud/\nu$, where p_2 is the absolute pressure

on the downstream side of the microbbuble generator orifice, p_v is the water vapour pressure, p_1 is the absolute pressure on the upstream side of the generator orifice, ρ is the water density, U is the generator jet mean velocity based on orifice throat area, d is the orifice diameter, S is the water surface tension and ν is the water kinematic viscosity. Table 1 shows a summary of the experimental parameters for the 10 runs made.

Saturation vessel absolute pressure, kPa	480.8
Saturation vessel water dissolved O_2 conc , ppm	48
Supersaturated water flow rate, mℓ/s	4.124
Dilution flow rate, mℓ/s	193.1
Microbble generator σ	0.30
Microbble generator We	2980
Microbble generator Re	9780

Table 1. Summary of relevant experimental parameters.

Bubble Recognition and Sizing

Shadowgraph analysis performed by the DaVis software produces a bubble size histogram. The recognition algorithm includes several criteria for validated particle detection. Validated particles are subsequently evaluated by the sizing algorithm to determine their diameter, whereby they are assigned to a size interval. The parameters developed for the present shadowgraph analysis are shown in table 2 for reference. A full discussion of this parameter set is beyond the scope of the present paper.

Image pre-processing	3×3 median smoothing filter
Reference image using strict sliding maximum filter	300 pixel length
Global threshold	35%
Low level threshold	40%
High level threshold	70%
Area of interest	75%
Max low level area% of high level area	260%
Minimum area	50 pixels
Minimum centricity	65%

Table 2. Summary of LaVision DaVis Ver. 7.2 [9] software particle sizing parameters based on [8].

The bubble production frequency was estimated for each size interval by multiplication of the bubble volumetric concentration and the total liquid volumetric flow rate. The bubble volumetric concentration for each size interval was derived from the bubble size histogram by division by an effective measurement volume. This volume was derived from the field of view of the imaging optics and an effective depth of field for the whole validation process. This depth of validation decreases linearly with decreasing particle diameter [8] and is the range of positions parallel to the optical axis where bubbles are validated by the recognition algorithm.

The depth of validation was calibrated by applying the sizing algorithm to 400 sequential images of multiple opaque disks, of known diameter sparsely separated on a glass reticule. This was traversed parallel to the optical axis in steps of 10 μm spanning ± 2 mm about the focal plane. The opaque disks had diameters ranging between 10 to 200 μm. The spacing between disks was used to scale the field of view. Further, before calculating the volumetric concentration the bubble size histogram was corrected to compensate for bubbles touching the borders of the image.

The uncertainty in the estimate of the mean bubble production frequency was calculated using the minimum and maximum values of each size interval. Other errors will be present due to performance of the sizing algorithm. The sequence of images acquired for calibrating the depth of validation were analysed to determine the maximum diameter deviation by comparison with

their true values. Also measured was the frequency of bubbles falsely validated or rejected. Particles falsely validated are those validated by the algorithm but lie outside of their calibrated measurement volume. Such particles were assigned diameters which were significantly less than their true value. The frequency of rejection of valid particles is influenced by local background noise due to the proximity of neighbouring bubbles.

Results

Raw data were obtained using the bubble recognition and sizing algorithm for each of the 10 runs. These data were then averaged and examined for statistical convergence. Figure 4 shows a waterfall plot of normalised histograms of microbubble diameter averaged for several running image sums. The diameter count is in 5 µm intervals plotted using the maximum value. The plot shows the data are effectively stationary about the dominant size interval of 25-30 µm and convergence favourably on the tail for larger diameters. For the total 5397 images 8584 bubbles were detected giving on average about 1.6 detections/image.
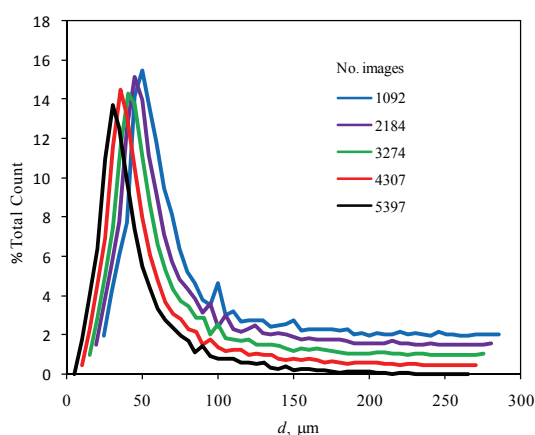

Figure 4. Waterfall plot showing convergence of raw normalised microbubble diameter histogram with number of acquired images. The 5 histograms shown correspond to running averages for 2, 4, 6, 8 and 10 runs each of about 545 images. The diameter count is in 5 µm intervals and plotted using the maximum value.

Figure 5 shows the production frequency histogram derived from the size histogram from 5397 images with border correction, depth of field applied and multiplied by the liquid volumetric flow as described above. From these results the total production frequency is about 469 kHz with a dominant size interval of 25-30 µm. The estimated microbubble volumetric concentration is 2.43/mm^3, the gas volumetric flow rate is 0.0329 mℓ/s and the void fraction is 0.017%.
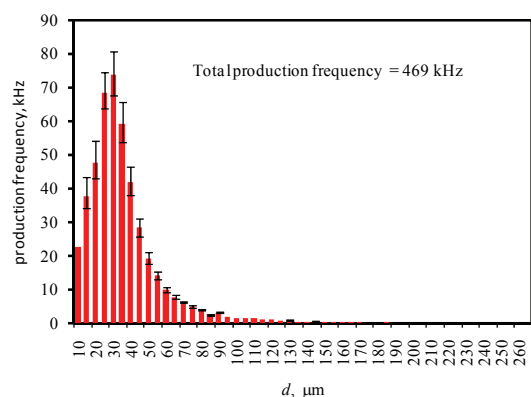

Figure 5. Microbubble production frequency histogram. The diameter frequency count is in 5 µm intervals and plotted using the maximum value. The error bars shown are based on uncertainties in the depth of field calculation due to size intervals chosen for the histogram.

Conclusions

An experimental setup and procedure have been developed for the measurement of microbubble size and production frequency using shadowography. The method provides essentially stationary data using about 5500 images giving on average about 1.6 detections/frame. The results of the measurements show that the mini-tube microbubble generator described, for the present test conditions, produces bubbles at a frequency of about 4.7×10^5 Hz with a dominant size range of 25-30 µm. Refinement of the method, further error analysis and testing of the microbubble generator under various conditions are the subject of ongoing work.

References

[1] Brandner, P.A., Walker, G.J., Niekamp, P.N. & Anderson, B., An Experimental Investigation of Cloud Cavitation about a Sphere, *J. Fluid Mech.*, **656**, 2010, 147-176.

[2] Brandner, P.A., Lecoffre, Y. and Walker, G.J., Development of an Australian National Facility for Cavitation Research, *Sixth International Symposium on Cavitation – CAV2006*, Wageningen, The Netherlands, 2006.

[3] Brandner, P.A., Lecoffre, Y. and Walker, G.J., Design Considerations in the Development of a Modern Cavitation Tunnel, *Sixteenth Australasian Fluid Mechanics Conference*, Gold Coast, Australia, 2007.

[4] Brennen, C.E., Cavitation in Biological and Bioengineering Contexts, *Fifth International Symposium on Cavitation – CAV2003*, Osaka, Japan, 2003.

[5] Brennen, C.E., *Cavitation and Bubble Dynamics*, Oxford University Press, 1995.

[6] Franc, J.P. & Michel J.M., *Fundamentals of Cavitation*, Kluwer Academic Publishers, 2004.

[7] Jeon, D., Graff, E. and Gharib, M., Measurement of Large Scale Bubbly Flows, *Twenty Seventh Symposium on Naval Hydrodynamics*, Seoul, Korea, 2008.

[8] Kim, S.K. and Kim, S.S, Drop Sizing and Depth of Field Correction in TV Imaging, *Atomiz. Sprays*, **4**, 1994, 65-78.

[9] LaVision GmbH, DaVis 7.2 Sizing Master Shadow Product Manual, 2009.

[10] Lecoffre, Y., *Cavitation Bubble Trackers*, A.A. Balkema, 1999.

[11] Lohse, D., Bubble Puzzles, *Physics Today*, **56**, 2003, 36-41.

[12] Sander, R., Compilation of Henry's Law Constants for Inorganic and Organic Species of Potential Importance in Environmental Chemistry, *Max–Planck Institute of Chemistry*, Online.

[13] Takahashi, T., Miyahara, T., & Mochizuki, H., Fundamental Study of Bubble Formation in Dissolved Air Pressure Flotation, *J. Chem Eng. Japan*, 1**2**, 1979, 275-280.

[14] Zimmerman, W.B., Tesar, V., Butler, S. & Bandulasena, H.C.H., Microbubble Generation, *Recent Patents on Engineering*, **2**, 2008, 1-8.